MDPI

Article

Water desalination using polyelectrolyte hydrogel: Gibbs ensemble modeling

Mikhail Laktionov [1,2], Lucie Nová [1] and Oleg V. Rud [1,3]*

[1] Department of Physical and Macromolecular Chemistry, Faculty of Science, Charles University in Prague, Czech Republic; e-mail@e-mail.com
[2] St. Petersburg National Research University of Information Technologies, Mechanics and Optics, St. Petersburg, Russia; e-mail@e-mail.com
[3] Institute of Macromolecular Compounds of Russian Academy of Sciences, Saint-Petersburg, Russia; e-mail@e-mail.com
* Correspondence: oleg.rud@natur.cuni.cz;

Abstract: Recently, polyelectrolyte hydrogels have been proposed as draw agents for forward osmosis (FO) desalination techniques. Indeed, polyelectrolyte hydrogels can absorb a big amount of water across an osmosis membrane as a result of their swelling pressure. On the other hand, the insoluble cross-linked hydrogel network enables dewatering under the influence of external (thermal and/or mechanical) stimuli. Moreover, from a thermodynamic perspective, the polyelectrolyte hydrogel is already an osmotic membrane. These above-mentioned hydrogel properties designate them as excellent candidates for desalination, and, at the same time, avoid the use of expensive membranes. In this article, we present our recent theoretical study of polyelectrolyte hydrogel usage for water desalination. Employing a coarse-grained model and the Gibbs ensemble, we modeled the thermodynamic equilibrium between coexisting gel phase and the supernate aqueous salt solution phase. We performed a sequence of step-by-step hydrogel compressions in *open* and *closed* systems. The compression in *open system* causes the decrease of salt ions inside the hydrogel, while the compression in *closed system* causes the decrease of the salt concentration in the supernatant solution. We modeled this stepwise process of continuous decrease of water salinity from seawater up to freshwater concentrations. We estimated the energy costs of the process to be comparable with reverse osmosis.

Keywords: polyelectrolye hydrogel; simulation; desalination

Citation: Lastname, F.; Lastname, F.; Lastname, F. Title. *Journal Not Specified* **2022**, *1*, 0. https://doi.org/

Received:
Accepted:
Published:

1. Introduction

«««< HEAD

The authors can follow the following references to generally highlight the global contamination and environmental pollution problems at the beginning of the introduction part https://doi.org/10.1016/j.jwpe.2022.102847 [1] https://doi.org/10.1016/j.ceramint.2022.05.151 [2] https://doi.org/10.3390/catal12050500 [3] https://doi.org/10.1007/s11356-022-21160-7 [4] https://doi.org/10.3390/ma15134547 [5] . Then, highlight the water desalination technologies and Gibbs ensemble (https://doi.org/10.3390/nano10020293 [6]).

Waste water treatment and technology is one of the greatest concerns of modern society. The waste water has to be disposed of both biological [4] and chemical [1,2] pollutants. Most imporatntly, water treatment technologies are needed for the still increasing demand on production of potable water from the brine, *i. e.* for desalination.

1.1. Water desalination technologies

Two basic approaches for separating water from salt are present in modern desalination technology [7,8].

The first approach is distillation, which uses heat to cause a phase change of the water to vapor. The vapor phase is separated from the brine and condenses to liquid fresh water. The released condensation energy is directed back to heat the feed solution. Distillation processes were the first desalination techniques conducted on a large commercial scale and still account for a large portion of the modern world's desalination capacity.

The second approach is to physically separate the brine components using an osmotic membrane transparent only for water molecules, which move in response to the difference in water chemical potential. In the context of our study, we will mention the reverse osmosis process (RO) as the major process of all the modern desalination industry, and the newly emerging membrane technology — forward osmosis (FO) [9]. In RO, the difference in water chemical potential originates from a difference in pressures applied to the feed and to product solutions. In FO, the chemical potential difference is due to an addition to solution from one side of the membrane (draw solution) the so-called draw solutes, which are lowering the water chemical potential in draw solution.

Distillation is easy and cheap technology but it is characterized by relatively high energy costs due to the dissipation of thermal energy. In turn, RO uses expensive osmotic membranes, which need to be replaced regularly because of scaling and fouling. Moreover, RO requires very high operating pressures, ranging from 20 to 200 bar, to let the water pass through the membrane. But, in terms of energy losses, it works close to the thermodynamic limit. Thus, theoretically, per one ion pair transferred from freshwater to salty water, it consumes only the energy equal to the difference between the chemical potentials of the transfered ions.

The absence of large hydraulic pressure in FO process (unlike in RO) allows to reduce the energy consumption in pumping, reduce membrane scaling and fouling, and therefore significantly increase the lifetime of the membranes. In FO, the draw solutes (agents) are dispersed and/or dissolved in water form homogeneous draw solutions. The correct choice of the draw agents is a task of paramount importance. As an osmotically driven process, the draw solute is expected to significantly reduce the water chemical potential, and consequently generate a high osmotic pressure. On the other hand, the draw solute is expected to be easily separated from water [10].

1.2. Hydrogels for desalination

Hydrogels are three-dimensional networks of polymer chains that are crosslinked by either physical or chemical bonds. They are able to entrap large volumes of water attracted by the high concentration of hydrophilic groups. When a dehydrated or deswollen hydrogel uptakes water, its polymer chains extend, creating a swelling pressure. For example, as reported in [11], weakly crosslinked poly(acrylic acid) (PAA) copolymers with polymer volume fractions between 0.03 and 0.30 exhibit a swelling pressure ranging from 0.20–4.23 MPa. Polyelectrolyte hydrogels, which are carrying ionic groups on the comonomer units (like PAA), are able to reject salt ions from the solution, they absorb a solution of lower salinity than that they are equilibrated with.

An important, advantageous aspect of polymer hydrogels is that they can undergo reversible volume change, *i. e.* solution — gel phase transitions in response to external stimuli. This aspect causes hydrogels to be labeled as 'smart' materials. Many physical and chemical stimuli have been applied to induce various responses of such smart hydrogels, in particular, to change them from hydrophilic to hydrophobic, thereby releasing water. The physical stimuli include: temperature, solvent composition, light, mechanical pressure, sound, electric and/or magnetic field, whilst the chemical (or biochemical) stimuli include pH, ionic strength, and specific molecular recognition [12–15].

Li *et al.*[16] took advantage of the smart hydrogel properties for desalination purposes. In this work, the authors used hydrogels as draw agents for FO. They have demonstrated

that the hydrogels are able to absorb water across the FO membrane due to their swelling and osmotic pressure and allow dewatering under the influence of stimuli (thermal and/or mechanical), due to their insoluble cross-linked polymer network. They have proposed the use of hydrogel based on thermoresponsive polyelectrolyte — copolymer of poly-N-isopropyl acrylamide (p-NIPAAm) and polyacrylic acid (p-AA). This gel network is either hydrophilic or hydrophobic, depending on the temperature. Such gel accumulates water inside the network in its hydrophilic state, but it releases the water out in its hydrophobic state.

From a thermodynamics perspective, the polyelectrolyte hydrogel itself is an osmotic membrane generating Donnan potential, which rejects ions between outer and inner solutions [17]. Such a view on hydrogels was employed in a series of works by the group of prof. Wilhelm (see for example [18,19]). The authors of these works proposed to get rid of the osmotic membrane and simply use only micro filtration to compress the hydrogel squeezing out the accumulated inside the gel solution. In their method, the deswollen hydrogel was first equilibrated with saline water feed. During the equilibration, the gel was swelling, absorbing the water. Then it was taken out from the feed solution and mechanically squeezed by means of a microfiltration membrane. They have found that the brine, which was squeezed out, had lower salinity than the feed water.

Similar approach was used by Ali *et al.*[20]. Here the authors used the thermosensitive gel (based on copolymers p-NIPAAm and p-AA), and instead of physical compression, the dewatering was done by an external heating stimulus (sunlight). The gel was equilibrated with feed water during the night, and, at daytime, under sunlight, the gel was shrinking and releasing the solution.

1.3. Physics behind the desalination process

Since the polyelectrolyte gel has its own charges and its own neutralizing counterions, the density of mobile ions (which are able to freely enter and leave the gel) inside the gel network appears to be smaller than their density outside the gel. Therefore the internal solution in the gel has lower density of mobile ions than the solution outside. In that sense, the gel acts as an osmotic membrane separating solutions [21]. The driving force of the separation is the Donnan potential, which originates from the charges in the hydrogel network. The difference between the densities (concentrations) of the mobile ions in the internal and external solutions is defined by Donnan law [22]

$$\frac{c^{\text{gel}}_{\text{Cl}^-}}{c_{\text{s}}} = \frac{c_{\text{s}}}{c^{\text{gel}}_{\text{Na}^+}} = \sqrt{1 + \left(\frac{\alpha}{2c_{\text{s}}V_{\text{gel}}}\right)^2} \pm \frac{\alpha}{2c_{\text{s}}V_{\text{gel}}} \tag{1}$$

where $c^{\text{gel}}_{\text{Cl}^-}$ and $c^{\text{gel}}_{\text{Na}^+}$ are the concentrations of monovalent anions and cations in the internal solution, c_{s} is the salinity of external solution, V_{gel} is the gel molar volume (inverse density of gel segments) and α is ionization degree (in the case of our study $\alpha = 1$). The $\pm$ sign in the formula accounts for the sign change for the cases of polyanion or polycation gels.

As shown in [18**? ?** ,19], the solution of lower salinity can be extracted from the gel by means of compression and/or other stimulus, provided that the charge in the gel remains constant. In the case of weak polyelectrolyte (pH-sensitive) gel, the compression discharges the gel and therefore the neutralizing counterions leave out the gel, diminishing the desalination effect [22].

One can argue that the sole Donnan effect is insufficient to achieve a high salt rejection [10] and the salinity of the water squeezed from hydrogel under a very high hydraulic pressure (up to 100 bar [19]) turns out to be not much different from the initial. Indeed, the use of high hydraulic pressure diminishes all the advantages of this method over RO, and the reversibility of hydrogel swelling after strong compression remains questionable. Nevertheless, in this study, we model the compression of the gel limiting ourselves to low compression rates, less than 5 bar, and studied how the compression of the gel affects the

surrounding salinity. We modelled the desalination process, as a cascade of step-by-step gel swellings and compressions, driving the salinity of the supernate down to potable water.

2. Model and methods

2.1. Open and closed sytems

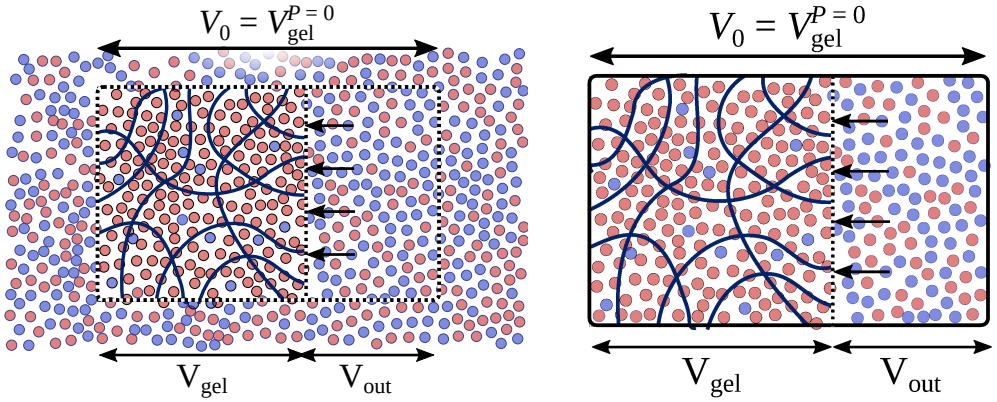

(a) Open system **(b)** Closed system

Figure 1. Diamond-like network in the simulation box. Color code represents the individual ion types (red: Na^+, blue: Cl^-, yellow: Ca^{2+}) and the hydrogel (grey: neutral segment (AH), cyan: charged segment (A^-)). .

We propose the desalination process as a cascade of gel compressions and decompressions lowering the supernatant salinity. In this process, the gel is supposed to be compressed/decompressed in an *open system* and in a *closed system*. The compression in *open system* assumes that the gel is in thermodynamic equilibrium with a huge (effectively **infinite**) reservoir of an aqueous solution, whereas the *closed system* implies that the gel is in equilibrium with a **finite** reservoir of an aqueous solution.

Due to huge size of the reservoir, the compression of the gel in *open system* does not affect the reservoir salinity, $c_s = c_{Na^+} = c_{Cl^-} = \text{Const}$, whereas the number of ions entrapped in the volume V_0 changes (Figure 1a). On the contrary, the compression of the gel in the *closed system* changes the salinity in the reservoir, but the total number of Na^+ and Cl^- ions in the gel and in the reservoir, *i. e.* in the volume V_0 (Figure 1b), remains constant.

The mechanical movement and the exchange of ions occur simulataneously in reality, however, we simulate them alternating each other in stop-run mode. To sample mechanical properties of the gel and reservoir we use MD simulation, whereas to sample the ions distribution between the gel and a reservoir we use MC simulation. The details of this hybryd MCMD computational technique can be found in our previous studies of polyelectrolytes in open system [21,23,24].

2.2. Langevin Dynamics

We model the gel as a network of 16 linear polymer chains, each consisting of 30 monomer units. These polymer chains are connected to a diamond-like network by 8 crosslinking units. This means, there are $N_{gel} = 16 \cdot 30 + 8 = 488$ gel monomers in the simulation box (see Figure 2). The network is put in simulation cubic box of the volume V_{gel} with periodic boundary conditions, which virtually emulaates an infinite polymer network.

Each monomer unit of the network carries a negative elementary electric charge. Except for the gel monomers, the monovalent co- and counter-ions ions, Cl^- and Na^+, are present in the simulation box. The total electric charge of all the particles in the box is zero, therefore the amount of Na^+ ions exceeds the amount of Cl^- by N_{gel}.

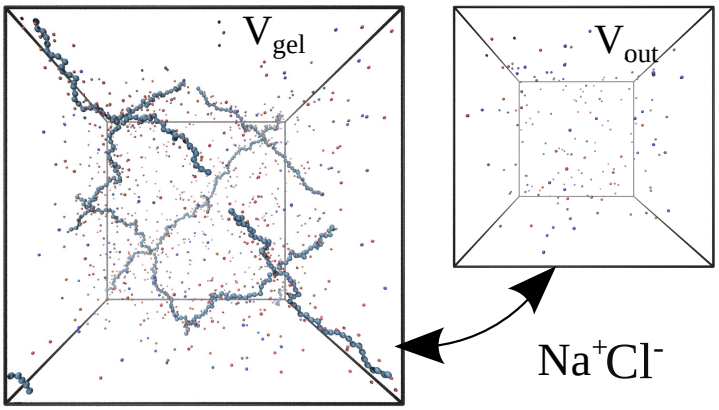

Figure 2. Diamond-like network in the simulation box. Color code represents the individual ion types (red: Na^+, blue: Cl^-, yellow: Ca^{2+}) and the hydrogel (gray: neutral segment (AH), cyan: charged segment (A^-)). .

Each pair of the particles interact via the truncated Lennard-Jones interaction potential, which imposes strong repulsion between all particles at short distances:

$$V_{\mathrm{LJ}}(r) = \begin{cases} 4\varepsilon\left(\left(\frac{\sigma}{r}\right)^{12} - \left(\frac{\sigma}{r}\right)^{6}\right) & \text{if } r < r_{\mathrm{cut}} \\ 0 & \text{elsewhere} \end{cases}, \tag{2}$$

where r is the interparticle distance, $\sigma = 0.35$nm is a chosen characteristic size of the particles, $\varepsilon = k_{\mathrm{B}}T$ is the depth of the potential and r_{cut} is the cut-off distance beyond which the potential is set zero.

The bonds connecting the gel to a network are modeled using finite extension nonlinear elastic potential (FENE)

$$V_{\mathrm{FENE}}(r) = -\frac{1}{2}K\Delta r_{\mathrm{max}}^2 \ln\left[1 - \left(\frac{r - r_0}{\Delta r_{\mathrm{max}}}\right)^2\right], \tag{3}$$

where r is the distance between the bonded segments, K is the magnitude of their interaction, Δr_{max} is the maximal stretching length of the bond and r_0 is the equilibrium bond length. For our simulations we chose $K = 10k_{\mathrm{B}}T/\sigma^2$, $\Delta r_{\mathrm{max}} = 2\sigma$ and $r_0 = 1.0\sigma$ [25].

All the charged paticles interact via Coulomb electrostatic potential:

$$V_{\mathrm{EL}} = l_{\mathrm{B}}k_{\mathrm{B}}T\frac{q_1 q_2}{r}, \tag{4}$$

where l_{B} is Bjerrum length; $l_{\mathrm{B}} = 2\sigma = 0.7$nm which corresponds to the Bjerrum length in water at temperature $T = 300$K, k_{B} — Botlzman constant. In that sense, the solvent (water) accounted for in the model implicitly via setting up dielectric permittivity $\epsilon = 80$.

We used Langevin thermostat, *i. e.* the two additional terms to force in equation of motion were added

$$\mathbf{f}_i = -\gamma\mathbf{v}_i(t) + \sqrt{2\gamma k_{\mathrm{B}}T}\boldsymbol{\eta}_i(t), \tag{5}$$

where the first term correspond to constant friction with γ being a friction coefficient, and the second one corresponds to random thermal force with $\boldsymbol{\eta}_i$ being a normally distributed random vector; $\mathbf{v}_i$ — velocity of i-th particle (see for details [26]).

2.2.1. Monte Carlo sampling in *open system*

Monte Carlo scheme for sampling the exchange of ions in *open system* is based on the formula for free energy of grand canonical ensemble.

$$\Omega_{\text{open}} = E - TS + \sum_i \mu_i N_i \tag{6}$$

where E is internal energy, T — temperature, S — entropy, N_i is the number of ions of type $i \in \{\text{Na}^+, \text{Cl}^-\}$, μ_i — corresponding chemical potential.

The entropy S is given by the Boltzmann formula [27]

$$S = k_{\text{B}} \sum_i \ln \frac{V_{\text{gel}}^{N_i}}{N_i!} \tag{7}$$

which accounts for two contributions:

1. the combinatorial entropy $S_c = -k_{\text{B}} \sum_i \ln N_i!$ which reflects the freedom of choice among the particles
2. the mixing entropy $S_m = k_{\text{B}} \sum_i N_i \ln V_{\text{gel}}$ which reflects the freedom to place the chosen particle randomly within the simulation box.

V_{gel} is the unitless volume, *i. e.* the volume measured in units of σ^3. Thus the change of free energy associated with an exchange of ion pairs is

$$\Delta\Omega_{\text{open}} = k_{\text{B}}T \ln \prod_i \left(V_{\text{gel}}^{\xi} \frac{N_i!}{(N_i + \xi)!} \right) + \xi \sum_i \mu_i + \Delta E \tag{8}$$

where ξ is an algebraic number of inserted (or removed) ion pairs; in general ξ can be any number, but in the case when $\xi = \pm 1$, which corresponds to addition or removal of only one ion pair, the Equation 8 gets simplified

$$\Delta\Omega_{\text{open}} = k_{\text{B}}T \ln V_{\text{gel}}^{2\xi} \prod_i (N_i + \theta(\xi))^{-\xi} + \xi \sum_i \mu_i + \Delta E \tag{9}$$

where θ is the Heaviside function, $\theta(\xi) = 1$, if $\xi = +1$, $\theta(\xi) = 0$, if $\xi = -1$.

The procedure of the Monte Carlo Sampling is the following [28]

1. propose the new configuration of the system by insertion (or deletion) of an ion pair, $\xi = \pm 1$
2. accept the new configuration if

$$\mathcal{R}^{\xi} < e^{\Delta\Omega_{\text{open}}/k_{\text{B}}T} = V_{\text{gel}}^{2\xi} \prod_i (N_i + \theta(\xi))^{-\xi} e^{(\Delta E + \xi\mu)/k_{\text{B}}T} \tag{10}$$

   where $\mathcal{R}$ is uniformly distributed random number in range between 0 and 1.
3. then collect the number of ions, N_{Na^+} and N_{Cl^-} to the samples array.

2.3. Monte Carlo sampling in closed system

In the *closed system* a the gel exchanges particles with explicit finite reservoir box. The total number of ion species in both boxes is fixed, whereas the density of ions in extrernal reservoir is defined by thermodynamic equilibrium between the two subvolumes (see Figure 1b. The Monte Carlo sampling of the distribution of ions between the subvolumes performed in a way similar to described in [29].

add here that citation about Gibbs ensemble

The free energy of the Gibbs ensemble is a sum of the gel's free energy and that of the external volume.

$$\Omega_{\text{closed}} = E_{\text{gel}} - TS_{\text{gel}} + E_{\text{out}} - TS_{\text{out}} \tag{11}$$

using similar reasoning as for *open system* one can derive the change of free energy associated with ion pair exchange

$$\Delta\Omega_{\text{closed}} = 2k_BT \ln\left(\frac{V_{\text{gel}}}{V_{\text{out}}}\right)^{\xi} \prod_i \left(\frac{N_i^{\text{gel}} + \theta(\xi)}{N_i^{\text{out}} + \theta(-\xi)}\right)^{-\xi} + \Delta E_{\text{gel}} + \Delta E_{\text{out}} \tag{12}$$

where ξ defines the direction of the trial move, so that $\xi = -1$ when an ion pair moved from gel to outside volume and $\xi = +1$ otherwise, ΔE_{gel} and ΔE_{out} are corresponding changes of the potential energy of the gel and the outside volumes.

Then the procedure of sampling is the same as that for *open sysytem*: (1) propose the move of an ion pair, (2) accept a new state if $\mathcal{R}^{\xi} < \exp(\Delta\Omega_{\text{closed}}/k_{\text{B}}T)$, (3) repeat the procedure until the desired number of samples is reached.

2.4. Algorithm

As mentioned above, the whole simulation run consists of MD and MC subsimulations of mechanical movement of the particles and ion exchange. The algorithm is following:

1. Initiate the systems to simulate: the gel of the volume V_{gel} and the external solution of the volume V_{out};
2. Equilibrate the system running interspersing the MD and MC stages
3. Run the MD subsimulation and collect the observables: pressure in both volumes, P_{gel}, P_{out}, and distancies between the nodes of the gel network. The last one needed to estimate the autocorrelation of MD simulation;
4. Run MC procedure simulating ion exchange and collect the number of ions in both boxes, $N_{\text{Cl}^-}^{\text{gel}}$ and $N_{\text{Cl}^-}^{\text{out}}$;
5. Repeat the MD and MC subsimulations until the desired length of sample arrays is reached.

Using the data obtained from simulations we calculate v_{gel} — molar volume of the gel, *i. e.* the volume of the gel per one mol of gel segments, $v_{\text{gel}} = V_{\text{gel}}/N_{\text{gel}}$; Π — partial pressure of the gel, *i. e.* the pressure that needs to be applied to the gel via a solvent permeable filter to compress the gel to a specific molar volume; c_{s} — the density of ions in the outside volume; and n_{Cl^-} — the total amount of the ions in both volumes divided by the total volume of both boxes, $n_{\text{Cl}^-} = N_{\text{Cl}^-}/V_0$

V_0 was chosen to be close to the gel free swelling equilibrium, that to the the state when $\Pi = 0$. In order to obtain the value V_0 we perform the set of open system simulations for various V_{gel}. That value of V_{gel}, at which Π is closest to zero we choose as V_0. Then as soon as V_0 is defined we perform the compression of the gel in closed system decreasing the V_{gel} starting from V_0 and correspondingly increasing the outer volume V_{out}.

We have the "Gibbs ensemble" in the title, and this term is not used in the manuscript at all. TODO concise description of Gibbs ensemble, solving the task to Reviewer 2, Q5 and Q7

3. Results and discussion

3.1. Compression in open system

So, at the beginning, we run a set of simulations modeling the gel compression in *open system*, *i. e.* in equilibrium with a big bath of certain salinity, c_{s}. The simulations were run for a set of different gel volumes, V_{gel}. Each simulation returned the averaged values of pressures, P_{gel}, and the number of Cl^- ions, present in the simulation box, $N_{\text{Cl}^-}^{\text{gel}}$.

In order to get the *partial pressure* of the gel, we subtracted from P_{gel} the osmotic pressure of ions in the reservoir: $\Pi = P_{\text{gel}} - P_{\text{out}}$. P_{out}, in turn, we obtained from a separate simulation of a reservoir, containing ionic gas in equilibrium with the bath of the same salinity c_{s}.

The dependencies of Π on V_{gel} for *open system* for a set of various salinities are presented in Figure 3a by solid lines. For example, the blue solid line illustrates the compression (or swelling) of the gel in equilibrium with a reservoir of salinity, $c_{\text{s}} = 0.063$ mol/l. The points where the pressure equals zero, $\Pi = 0$, (indicated by filled circles) are the gel *free swelling equilibrium* states. These states are characterized by the corresponding molar vol-

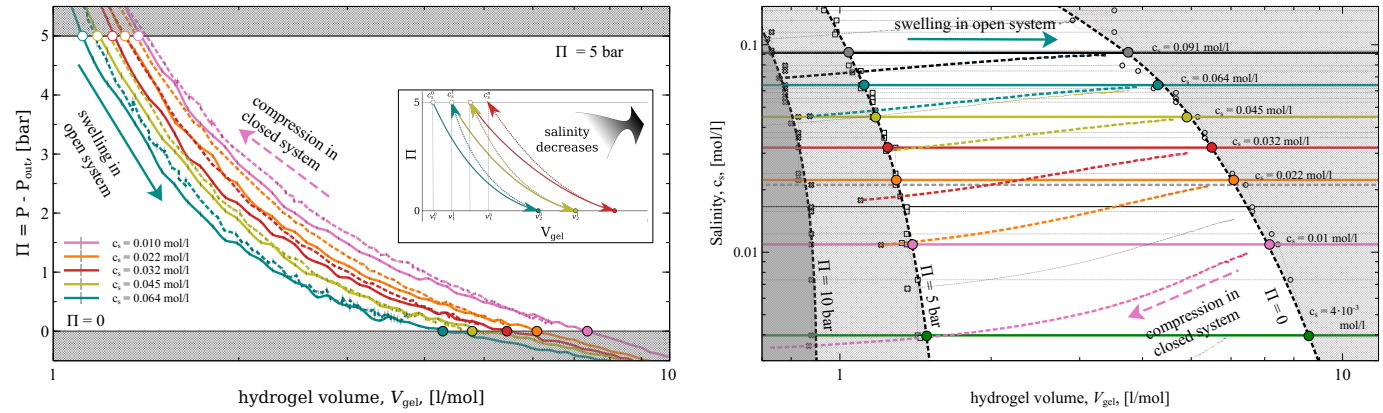

(a) The gel partial pressure vs gel molar volume

(b) Supernate salinity vs gel molar volume

Figure 3. The compression of the gel in the *open system* (solid lines) and in the *closed system* (dotted lines). Each solid curve corresponds to different salinity of the reservoir c_s (see legend). The shadowed areas limit the states with applied pressure below zero and above 5 bar.

ume of the gel, V^0_{gel} and the amount of ions in gel $\{N^0_{Na^+}, N^0_{Cl^-}\}$ (Index "0" stands for zero bar applied pressure). The *free swelling equilibrium* states' positions shift towards smaller volumes with increase of salinity. In general, the increase of salinity shifts all the $\Pi(V)$ curves towards smaller volumes. This effect is well known and is typical for all branched *strong* polyelectrolytes. It is caused by the decrease of ions osmotic pressure and by a screening of electrostatic interactions [24,30]. (The salinity dependence of the size of *weak* polyelectrolyte gel is in general non-monotonic. We discuss this case in [22].)

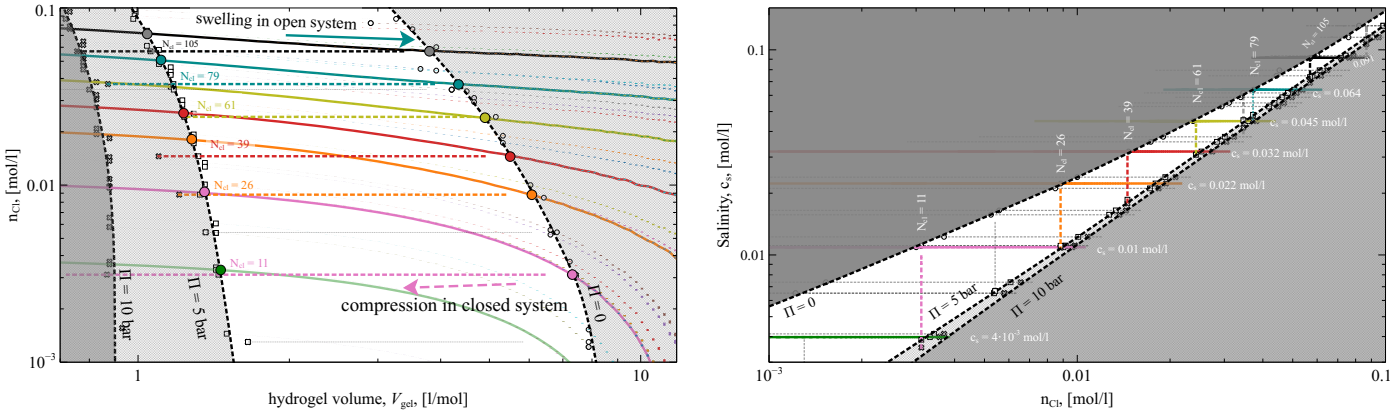

(a) Pressure vs gel molar volume

(b) Salinity vs gel molar volume

Figure 4. The compression of the gel in *open system* (solid lines) and in *closed system* (dotted lines). Shadowed area limit the states with applied pressure below zero and above 5 bar. The values N_{Cl^-} are the virtual numbers of present Cl^- ions in *closed system* simulation boxes.

3.2. Compression in closed system

The simulations in *closed systems* start from the V^0_{gel} and $\{N^0_{Na^+}, N^0_{Cl^-}\}$ values obtained from the corresponding *open system* simulations. The simulation of gel compression in a closed volume, V_0, starts at the point $V_0 = V^0_{gel}$, and ion content $N^0_{Cl^-}$ for Cl^- ions. The Na^+ ions amount is neutralize the system, $N^0_{Na^+} = N^0_{Cl^-} + N_{gel}$.

We prepare two systems: one for simulation of the gel at the volume V_{gel}, and the other one for simulation of the supernatant solution at the volume $V_{\text{out}} = V_0 - V_{\text{gel}}$. Note that the ions of the amount $N^0_{\text{Cl}^-}$ and $N^0_{\text{Na}^+}$ are shared by the two volumes.

The processes of the gel compression in *closed system* are depicted in Figure 3a as dotted lines. In this plot, for example, the blue dotted line illustrates the compression of the gel equilibrated with the solution of salinity $c_s = 0.063$ mol/l at volume, at which the gel has at zero pressure. The volume values V_{gel} and V_{out} are comparable in the *closed system* case. Therefore, the gel compression causes decrease of the salinity in the supernate, c_s. This dependence is illustrated in Figure 3b, where the same swelling/compression processes are displayed in different coordinates: *i. e.* salinity of supernate versus the gel molar volume, $c_s(V_{\text{gel}})$. In these coordinates, all the open system compressions show up as horizontal lines, which reflects the constant salinity, whereas the compressions in closed system demonstrate the change of c_s from $c^0_s = 0.063$ at zero pressure Π to $c^5_s = 0.045$ mol/l at $P^{\text{gel}} = 5$ bar (index "5" stands for 5 bar).

Although the salinity during compression in *open system* remains constant, the amount of ions in the compressed subsystem (*i. e.* in the volume where the gel is compressed (or swells)), changes. Here, the compression volume V_0 is the volume of the *free swelling equilibrium* state of the gel, $V_0 = V^0_{\text{gel}}$. Figure 4a shows number of Cl^- ions in the volume V_0 per unit volume, $n_{Cl^-} = N_{Cl^-}/V_0$, as a function of the gel molar volume. The depicted values can be considered as the average density of Cl^- ions in the compression volume V_0.

The n_{Cl^-}-V_{gel} dependencies look like horizontal lines in the case of *closed system* compression, whereas n_{Cl^-} increases with V_{gel} during the compression in the *open system* case. This implies, that the compression of the gel in the *open system* pulls out the ions from the bath to the compression volume, V_0. And vice versa, the swelling of the gel pushes ions out to the bath.

Finally, the same processes are depicted in Figure 4b in coordinates n_{Cl^-} — c_s. In these coordinates, both ways of the compression, in *open* and in *closed* systems, appear as straight vertical and horizontal lines correspondingly.

In our study, we modeled the compression of the gel in equilibrium with reservoirs of 40 different salinities, ranging from 0.001 to 0.5 mol/l. The *open system* compressions resulted in a defined free swelling equilibrium states, which we used as the initial conditions for the respective compressions in *closed systems*. All the corresponding dependencies are depicted in Figures 3 and 4 as thin grey dashed lines (some of them are highlighted and colored). The states corresponding to $P^{gel} = 0$, 5 and 10 bar pressure are marked by open circles, squares, and crosses respectively. The non-shadowed areas in the Figures highlight the states in which the gel partial pressure ranges between the experimentally relevant values, 0 and 5 bar.

3.3. Desalination scheme

It follows that the compression of the gel in the *closed system* affects the salinity, whereas the compression in the *open system* affects the amount of ions in the gel subsystem. Here we show how to employ these phenomena for water desalination. The highlighted colored lines on plots of Figures 3 and 4 form a sequence gel swellings and compressions, following one by one, correspondingly in *open* and *closed* systems. This sequence forms the water desalination process. Starting from swelling the gel in the *open system* at high salinity ($c_s = 0.091$ mol/l, solid black line), the gel is compressed in the *closed system* until the pressure reaches 5 bar (dashed black line). Then the same gel swells in a reservoir of a bit lower salinity in the *open system* (*i. e.* $c_s = 0.064$ mol/l, light blue line). After the swelling, the gel is compressed again with the pressure 5 bar in *closed system* (dashed light blue line). Then the gel swells in a reservoir of even smaller salinity ($c_s = 0.045$ mol/l, solid yellow line), and so on. This chain of alternating swellings and compressions ends up when salinity is equal to $c_s = 4 \cdot 10^{-3}$ mol/l after the compression in the *closed system* (dashed magenta line).

The plots in Figures 3 and 4 depict the whole process in all possible coordinate representations. In all plots, the lines corresponding to sequential swellings and compressions during the whole desalination process resemble a 'pathway'. In particular, the desalination process depicted in Figure 4b resembles a staircase, where the *open system* processes are horizontal lines and the *closed system* processes are vertical lines.

3.4. The efficiency of desalination

The theoretical minimum specific energy for seawater desalination ($c_s \simeq 0.6$ mol/l as for pure NaCl) is ~ 3.9 kJ/l (1.1 kWh/m^3) for 50% recovery [31]. This value is calculated as follows

$$W = 2RT\left(\frac{c_f}{R_w}\ln\frac{c_b}{c_f} - c_p \ln\frac{c_b}{c_p}\right) \tag{13}$$

where R is a universal gas constant, c_f is the salinity of feed water, c_p is the salinity of product water and c_b is the salinity of the brine, which necessarily appears in any desalination process. R_w is a recovery ratio, *i. e.* the ratio between volume of produced water and the volume of the feed water. 50% recovery ratio means that one part of feed water divides into two equal volume solutions of the product water and of the brine. Of course, a significant amount of additional energy is required to operate the system[32]. It has been reported that the specific energy consumption (SEC) of reverse osmosis (RO) process is 2.5 – 4.0 kWh/m3 (9 – 14.4 kJ/l), which is significantly higher than its minimum specific energy. The SEC of a real-scale RO plant is even higher, approximately 3.5 – 4.5 kWh/m^3 (12.6 - 16.2 kJ/L), including pre-treatment and post-treatment processes [33].

In order to compare the efficiency of the process presented in 3 and 4 with provided values, we collect the corresponding data to the Table 1. The presented desalination process is a cascade of six swellings in open system, at six different (constant) salinities c_s, each followed by six compressions in closed system, at six different (constant) n_{Cl^-}. Each swelling and compression process is presented as a row of Table 1, which is colored by matching the lines in the Figures. The first column of the table contains values c_s^0 and c_s^5, which stand for the supernate salinity at 0 and 5 bar compression; in open system, supernate salinity does not change, so c_s^0 and c_s^5 are presented by a single number. The second column contains values of n^0 and n^5, which stand for the number of Cl^- ions in compression volume V_0, at 0 and 5 bar pressure (divided by V_0). The number of ion does not change in closed system compression, thus n^0 and n^5 are the same in the corresponding rows. The third column shows the change of the gel volume in corresponding process, Δv. The fourth column contains the work needed for the compression in the corresponding process per volume of extracted solution. This value is an integral of corresponding $\Pi(V_{gel})$ dependence [34]

$$W = \frac{\int_{v^0}^{v^5} \Pi dV_{gel}}{\Delta v} \tag{14}$$

the equation must be supported by referrence

Here, in the table, we present the absolute values of the work, whereas one should keep in mind that the compression implies the work is done by external force and the swelling implies that the work is done by gel.

To give a clue of comparison with ideal desalination process efficiency, the fifth column provides the values of specific energy consumption, W^{id}, which are calculated by means of Equation 13, using the following procedure: Let§s assume the concentration of the feed solution to be $c_s^f = 44.91$ mmol/l and the concentrations of product and brine solutions to be $c_s^p = 31.93$ mmol/l and $c_s^b = 63.93$ mmol/l, respectively.

1. The gel, equilibrated with the feed solution, is compressed in the *closed system*. The gel volume decreases by $\Delta v^p = 3.69$ liters and the salinity of supernate decreases from c_s^f to c_s^p. The volume of the product solution is Δv^p
2. The squeezed gel is put back into the feed solution and is quilibrated there under pressure, so it does not swell.

Table 1. The estimates of the efficiency of the desalination process. All the units are calculated per one mol of gel segments. Values in brackets are the estimates corresponding to crossection of 'red' and 'orange' lines on the plots of Figures 3 and 4

c_s^0, mM	c_s^5, mM	$n^0_{Cl^-}$, mM	$n^5_{Cl^-}$, mM	ΔV_{gel}, l	$\lvert W \rvert$, J/l	W^{id}, J/l
91.47		$57.08 \pm 0.122 \longrightarrow 71.75 \pm 0.024$		2.74	95.4 ± 1.9	
$89.41 \pm 0.23 \longrightarrow 73.63 \pm 0.03$		56.90		2.72	109.1 ± 1.7	
63.93		$37.28 \pm 0.08 \longrightarrow 50.579 \pm 0.013$		3.26	100.9 ± 1.7	
$62.05 \pm 0.15 \longrightarrow 48.21 \pm 0.02$		37.17		3.18	107.4 ± 1.4	
44.91		$23.75 \pm 0.06 \longrightarrow 35.911 \pm 0.010$		3.82	106.7 ± 1.5	
$43.46 \pm 0.12 \longrightarrow 30.795 \pm 0.008$		24.27		3.91	106.4 ± 1.1	
31.93		$14.66 \pm 0.04 \longrightarrow 25.297 \pm 0.006$		4.20	107.9 ± 1.4	
$30.03 \pm 0.08 \longrightarrow 18.585 \pm 0.004$ (22.32)		14.55		4.17 (3.22)	115.6 ± 0.9 (57.3)	
22.30		$8.84 \pm 0.03 \longrightarrow 17.945 \pm 0.004$ (14.56)		4.75 (3.76)	108.1 ± 1.3 (68.3)	
$20.74 \pm 0.06 \longrightarrow 11.082 \pm 0.002$		8.83		4.71	110.8 ± 0.8	
10.90		$3.00 \pm 0.01 \longrightarrow 9.011 \pm 0.002$		6.08	106.9 ± 1.1	
$9.83 \pm 0.05 \longrightarrow 3.862 \pm 0.001$		3.12		5.78	119.4 ± 1.0	

$W^{sim} = 202.8 \pm 3.2$, $W^{id} = 52.9$, $R_w = 0.54$

$W^{sim} = 222.3 \pm 2.5$, $W^{id} = 43.8$ (41.0), $R_w = 0.52$ (0.46)

$W^{sim} = 227.5 \pm 2.3$, $W^{id} = 69.7$, $R_w = 0.55$

$W^{sim} = 207.3 \pm 2.2$, $W^{id} = 38.2$, $R_w = 0.53$

$W^{sim} = 218.7 \pm 2.2$, $W^{id} = 66.6$ (22.0), $R_w = 0.53$ (0.49)

3. After the equilibration, the gel swells in the *closed system* and the salinity of the external solution increases to the value c_s^b.
4. Finally, the gel is taken out and compressed by 5 bar in the *open system* in equilibrium with the brine bath. The change of the gel volume in this process is $\Delta v^b = 3.26$ l/mol, which equals to the volume of the produced brine.

Thus the recovery ratio $R_w = \Delta v^p/(\Delta v^p + \Delta v^b) \simeq 0.53$ and the theoretical minimum specific energy of the desalination process with corresponding c_s^f, c_s^p and c_s^b is $W^{id} = 38.2$ J/l (Equation 13).

The estimated W^{id} values are provided in the fifth column of the table, for five triplets of c_s^f, c_s^p,c_s^b values . W_{sim} is the energy calculated by integration of $\Pi(V_{\text{gel}})$ dependencies as the sum of corresponding compressions in *closed* and *open* systems, W_{id} is the estimation based on the equation Equation 13 and R_w is the corresponding recovery ratio. Note that calculating the W_{sim} we accounted for only the work done on the gel during the compression, whereas the work done by the gel itself during swelling was not taken into account. The ratio between W_{sim} and W_{id} ranges from 3.26 to 5.43, which is comparable to that of RO.

how the integration was performed

3.5. Study limitations

Like other simulation based studies, our research has a limited validity, primarily resulting from the simplifications applied in the used model. For example, our coarse-grained model cannot differentiate polystyrene sulphonate gel from other strong polyacidic gels. However, these limitations are also the advantage of our model because the results of our study can be applied to similar systems, including polybasic gels with all the charges reversed.

3.6. Implications and future perspectives

We are aware that the concept introduced in this simulation study need to be experimentally verified. Therefore, in the future, we want to focus on experimental aspects of desalination based on polyacidic gel compression.

4. Conclusions

We have modeled the compression of the polyelectrolyte gel in thermodynamic equilibrium with the supernatant aqueous solution of a limited amount. We have shown that the compression of the gel decreases the supernatant salinity. We employed this phenomenon for modeling the process of water desalination. The desalination was done as a sequential combination of two processes: (1) swelling of the gel in *open system*, exchanging ions with a big reservoir at constant salinity; (2) compression of the gel in *closed system*, when the gel exchanges ions with a small reservoir affecting its salinity. We estimated the energy consumption needed for producing one liter of potable water from brine and have shown that the proposed gel compression method may compete with modern desalination technologies.

Author Contributions: Conceptualization, O.R. ; methodology, M.L.; software, M.L.; validation, M.L., L.N. and O.R.; formal analysis, L.N.; data curation, M.L.; writing—original draft preparation, O.R.; writing—review and editing, L.N.

Funding: "This research was funded by Czech Science Foundation grant number 19-17847Y" and Government of Russian Federation grant number 14.W03.31.0022.

Acknowledgments: This research was supported by the Czech Science Foundation (grant 19-17847Y) Government of Russian Federation, grant number 14.W03.31.0022.

Conflicts of Interest: The authors declare no conflict of interest.

References

1. Baaloudj, O.; Badawi, A.K.; Kenfoud, H.; Benrighi, Y.; Hassan, R.; Nasrallah, N.; Assadi, A.A. Techno-economic studies for a pilot-scale Bi12TiO20 based photocatalytic system for pharmaceutical wastewater treatment: From laboratory studies to commercial-scale applications. *Journal of Water Process Engineering* **2022**, *48*, 102847. doi:10.1016/j.jwpe.2022.102847.
2. Shahzad, W.; Badawi, A.K.; Rehan, Z.A.; Khan, A.M.; Khan, R.A.; Shah, F.; Ali, S.; Ismail, B. Enhanced visible light photocatalytic performance of Sr0.3(Ba,Mn)0.7ZrO3 perovskites anchored on graphene oxide. *Ceramics International* **2022**, *48*, 24979–24988. doi:10.1016/j.ceramint.2022.05.151.
3. Baaloudj, O.; Kenfoud, H.; Badawi, A.K.; Assadi, A.A.; El Jery, A.; Assadi, A.A.; Amrane, A. Bismuth Sillenite Crystals as Recent Photocatalysts for Water Treatment and Energy Generation: A Critical Review. *Catalysts* **2022**, *12*. doi:10.3390/catal12050500.
4. Guesmi, A.; Cherif, M.M.; Baaloudj, O.; Kenfoud, H.; Badawi, A.K.; Elfalleh, W.; Hamadi, N.B.; Khezami, L.; Assadi, A.A. Disinfection of corona and myriad viruses in water by non-thermal plasma: a review. *Environ Sci Pollut Res* **2022**, *29*, 55321–55335. doi:10.1007/s11356-022-21160-7.
5. Kane, A.; Assadi, A.A.; El Jery, A.; Badawi, A.K.; Kenfoud, H.; Baaloudj, O.; Assadi, A.A. Advanced Photocatalytic Treatment of Wastewater Using Immobilized Titanium Dioxide as a Photocatalyst in a Pilot-Scale Reactor: Process Intensification. *Materials* **2022**, *15*. doi:10.3390/ma15134547.
6. Erdos, M.; Galteland, O.; Bedeaux, D.; Kjelstrup, S.; Moultos, O.A.; Vlugt, T.J.H. Gibbs Ensemble Monte Carlo Simulation of Fluids in Confinement: Relation between the Differential and Integral Pressures. *Nanomaterials* **2020**, *10*, 293. doi:10.3390/nano10020293.
7. Miller, J. Review of Water Resources and Desalination Technologies. Technical report, 2003. doi:10.2172/809106.
8. Curto, D.; Franzitta, V.; Guercio, A. A Review of the Water Desalination Technologies. *Applied Sciences* **2021**, *11*, 670. doi:10.3390/app11020670.
9. Akther, N.; Sodiq, A.; Giwa, A.; Daer, S.; Arafat, H.A.; Hasan, S.W. Recent advancements in forward osmosis desalination: A review. *Chemical Engineering Journal* **2015**, *281*, 502–522. doi:10.1016/j.cej.2015.05.080.
10. Cai, Y.; Hu, X.M. A critical review on draw solutes development for forward osmosis. *Desalination* **2016**, *391*, 16–29. doi:10.1016/j.desal.2016.03.021.
11. Wack, H.; Ulbricht, M. Effect of synthesis composition on the swelling pressure of polymeric hydrogels. *Polymer* **2009**, *50*, 2075–2080. doi:10.1016/j.polymer.2009.02.041.
12. Tanaka, T.; Nishio, I.; Sun, S.T.; Ueno-Nishio, S. Collapse of Gels in an Electric Field. *Science* **1982**, *218*, 467–469. doi:10.1126/science.218.4571.467.
13. Serizawa, T.; Wakita, K.; Akashi, M. Rapid Deswelling of Porous Poly(N-isopropylacrylamide) Hydrogels Prepared by Incorporation of Silica Particles. *Macromolecules* **2001**, *35*, 10–12. doi:10.1021/ma011362+.
14. Lietor-Santos, J.J.; Sierra-Martin, B.; Vavrin, R.; Hu, Z.; Gasser, U.; Fernandez-Nieves, A. Deswelling Microgel Particles Using Hydrostatic Pressure. *Macromolecules* **2009**, *42*, 6225–6230. doi:10.1021/ma9010654.
15. Qiu, Y.; Park, K. Environment-sensitive hydrogels for drug delivery. *Advanced Drug Delivery Reviews* **2001**, *53*, 321–339. doi:10.1016/s0169-409x(01)00203-4.
16. Li, D.; Zhang, X.; Yao, J.; Simon, G.P.; Wang, H. Stimuli-responsive polymer hydrogels as a new class of draw agent for forward osmosis desalination. *Chem. Commun.* **2011**, *47*, 1710. doi:10.1039/c0cc04701e.
17. Wang, H.; Wei, J.; Simon, G.P. Response to Osmotic Pressure versus Swelling Pressure: Comment on "Bifunctional Polymer Hydrogel Layers As Forward Osmosis Draw Agents for Continuous Production of Fresh Water Using Solar Energy". *Environmental Science and Technology* **2014**, *48*, 4214–4215. doi:10.1021/es5011016.
18. Arens, L.; Albrecht, J.B.; Höpfner, J.; Schlag, K.; Habicht, A.; Seiffert, S.; Wilhelm, M. Energy Consumption for the Desalination of Salt Water Using Polyelectrolyte Hydrogels as the Separation Agent. *Macromol. Chem. Phys.* **2017**, *218*, 1700237. doi:10.1002/macp.201700237.
19. Fengler, C.; Arens, L.; Horn, H.; Wilhelm, M. Desalination of Seawater Using Cationic Poly(acrylamide) Hydrogels and Mechanical Forces for Separation. *Macromol. Mater. Eng.* **2020**, *305*, 2000383. doi:10.1002/mame.202000383.
20. Ali, W.; Gebert, B.; Hennecke, T.; Graf, K.; Ulbricht, M.; Gutmann, J.S. Design of Thermally Responsive Polymeric Hydrogels for Brackish Water Desalination: Effect of Architecture on Swelling, Deswelling, and Salt Rejection. *ACS Appl. Mater. Interfaces Applied Materials and Interfaces* **2015**, *7*, 15696–15706. doi:10.1021/acsami.5b03878.
21. Rud, O.V.; Landsgesell, J.; Holm, C.; Košovan, P. Modeling of weak polyelectrolyte hydrogels under compression – Implications for water desalination. *Desalination* **2021**, *506*, 114995. doi:10.1016/j.desal.2021.114995.
22. Rud, O.; Borisov, O.; Košovan, P. Thermodynamic model for a reversible desalination cycle using weak polyelectrolyte hydrogels. *Desalination* **2018**, *442*, 32–43. doi:10.1016/j.desal.2018.05.002.
23. Rud, O.V.; Kazakov, A.D.; Nova, L.; Uhlik, F. Polyelectrolyte Hydrogels as Draw Agents for Desalination of Solutions with Multivalent Ions. *Macromolecules* **2022**, *55*. doi:10.1021/acs.macromol.1c02266.
24. Landsgesell, J.; Hebbeker, P.; Rud, O.; Lunkad, R.; Košovan, P.; Holm, C. Grand-Reaction Method for Simulations of Ionization Equilibria Coupled to Ion Partitioning. *Macromolecules* **2020**, *53*, 3007–3020. doi:10.1021/acs.macromol.0c00260.
25. Jin, S.; Collins, L.R. Dynamics of dissolved polymer chains in isotropic turbulence. *New Journal of Physics* **2007**, *9*, 360. doi:10.1088/1367-2630/9/10/360.
26. Grest, G.S.; Kremer, K. Molecular dynamics simulation for polymers in the presence of a heat bath. *Physical Review A* **1986**, *33*, 3628–3631. doi:10.1103/PhysRevA.33.3628.

27. Nagle, J.F. Regarding the Entropy of Distinguishable Particles. *Journal of Statistical Physics* **2004**, *117*, 1047–1062. doi:10.1007/s10955-004-5715-5.
28. Frenkel, D.; Smit, B. *Understanding Molecular Simulation*; Academic Press, San Diego, 2002.
29. Panagiotopoulos, A.; Quirke, N.; Stapleton, M.; Tildesley, D. Phase equilibria by simulation in the Gibbs ensemble. *Molecular Physics* **1988**, *63*, 527–545. doi:10.1080/00268978800100361.
30. Zhulina, E.; Klein Wolterink, J.; Borisov, O. Screening Effects in a Polyelectrolyte Brush: Self-Consistent-Field Theory. *Macromolecules 23 (2000). - ISSN 0024-9297* **2000**, *33*. doi:10.1021/ma990187i.
31. Wang, L.; Violet, C.; DuChanois, R.M.; Elimelech, M. Derivation of the Theoretical Minimum Energy of Separation of Desalination Processes. *Journal of Chemical Education* **2020**, *97*, 4361–4369. doi:10.1021/acs.jchemed.0c01194.
32. Kim, J.; Park, K.; Yang, D.R.; Hong, S. A comprehensive review of energy consumption of seawater reverse osmosis desalination plants. *Applied Energy* **2019**, *254*, 113652. doi:10.1016/j.apenergy.2019.113652.
33. Kim, J.; Hong, S. A novel single-pass reverse osmosis configuration for high-purity water production and low energy consumption in seawater desalination. *Desalination* **2018**, *429*, 142–154. doi:10.1016/j.desal.2017.12.026.
34. Atkins, P.; de Paula, J. *Physical Chemistry, Ninth Edition*; Oxford University Press, New York, 2010.